Geophys. J. Int. (2006) **165,** 991–1002 doi: 10.1111/j.1365-246X.2006.02900.x

Mechanical modelling of oblique convergence in the Zagros, Iran

Philippe Vernant* and Jean Chéry

Laboratoire Dynamique de la Lithosphère, CNRS-Université de Montpellier II, CC 060, *place E. Bataillon,* 34095 *Montpellier Cedex* 05, *France.*
E-mail: jean@dstu.univ-montp 2.fr

Accepted 2006 January 7. Received 2005 October 28; in original form 2005 October 28

SUMMARY

Recent GPS surveys indicate that the Zagros kinematics corresponds to an oblique convergence between a rigid central Iranian plateau and the Arabian plate at ∼7 mm yr^{-1} at the longitude of the Persian Gulf. Convergence is almost frontal in the SE Zagros and oblique (45°) in the NW part of the range. It has been proposed that internal deformation of the NW Zagros occurs in a partitioned mode. In such a view, the Main Recent Fault (MRF) bordering the Iranian plateau accommodates all the tangential motion, while shortening happens by pure thrusting within the fold and thrust belt as suggested by the focal mechanisms within the range. We use a 2.5-D mechanical finite element model of the Zagros to understand the influence on the Zagros deformation of (1) the obliquity of convergence, (2) the rheological layering of the lithosphere (strong upper crust, weak lower crust, strong or weak uppermost mantle) and (3) a possible weakness of the MRF. Surprisingly, a fully partitioned mode occurs only when the collision is very oblique. In the case of the NW Zagros, we find that the MRF can accommodate only ∼25 per cent of the whole tangential motion. As the GPS inferred range parallel motion across the NW Zagros is ∼5 mm yr^{-1}, the present day slip rate of this fault could be as low as 1.2 mm yr^{-1}. In agreement with the observed strain in SE Zagros, our model predicts that no strike-slip activity takes place on a vertical fault when the direction of convergence is more frontal. We discuss the implications of our model on the seismicity and kinematics of oblique collision zones by comparing our results with the available data in the Zagros and other oblique convergence domains.

Key words: fault model, finite-element methods, lithospheric deformation, orogeny, rheology.

INTRODUCTION

Two end-member models have been proposed to accommodate oblique convergence. In the first scenario (wrenching), the parallel and normal velocities vary more or less linearly across the deformation zone (Wilcox *et al.* 1973). In the second model, the deformation is partitioned into two components: the shortening component which is taken up by a dipping fault and the shear component, which occurs on a subvertical strike-slip fault (Fitch 1972). Partitioning has been often used to describe the localized deformation occurring in oblique subduction zones (McCaffrey 1992). It has also been proposed to describe the deformation mode within some of the accretionary prisms (Platt 1993). However, except for the study of Braun & Beaumont (1995), less quantitative work has been done on the strain partitioning in the framework of intracontinental oblique shortening (Krantz 1995; Teyssier & Tikoff 1998). In this paper, we study by means of mechanical modelling how oblique shortening is accommodated by the Zagros Mountains. We also further discuss the implications of our model in the understanding of other oblique convergence zones.

Zagros is part of the Iranian mountains which are actively deforming due to the shortening between Arabian and Eurasian plates (Fig. 1). Based on recent geologic and geodetic estimates the motion of Arabia with respect to a stable Eurasia has been estimated to ∼20 mm yr^{-1} with a north direction at the longitude of the Persian gulf (50–55° E) (Sella *et al.* 2002; McQuarrie *et al.* 2003; Vernant *et al.* 2004). This convergence is accommodated almost entirely in the Alborz (6–8 mm yr^{-1}) and Zagros Mountains (6–9 mm yr^{-1}), the remaining deformation being located somewhere in the south Caspian basin. As previously proposed on the base of the seismicity. (Jackson & McKenzie 1984) and recently confirmed by geodetic measurements (Vernant *et al.* 2004), central Iran does not significantly deform and acts as a backstop of the Zagros Mountains. Since the central Iranian block (CIB) moves at 13 mm yr^{-1} to the north relative to Eurasia, the relative velocity between the CIB and the Arabian plate is ∼7 mm yr^{-1} in a North-South direction. Because the main structural trend of Zagros is NW–SE (parallel to the plate

*Now at: Earth, Atmospheric and Planetary Sciences Department, Massachusetts Institute of Technology, 54-617, 77 Massachusetts avenue, Cambridge, MA 02139-4307, USA.

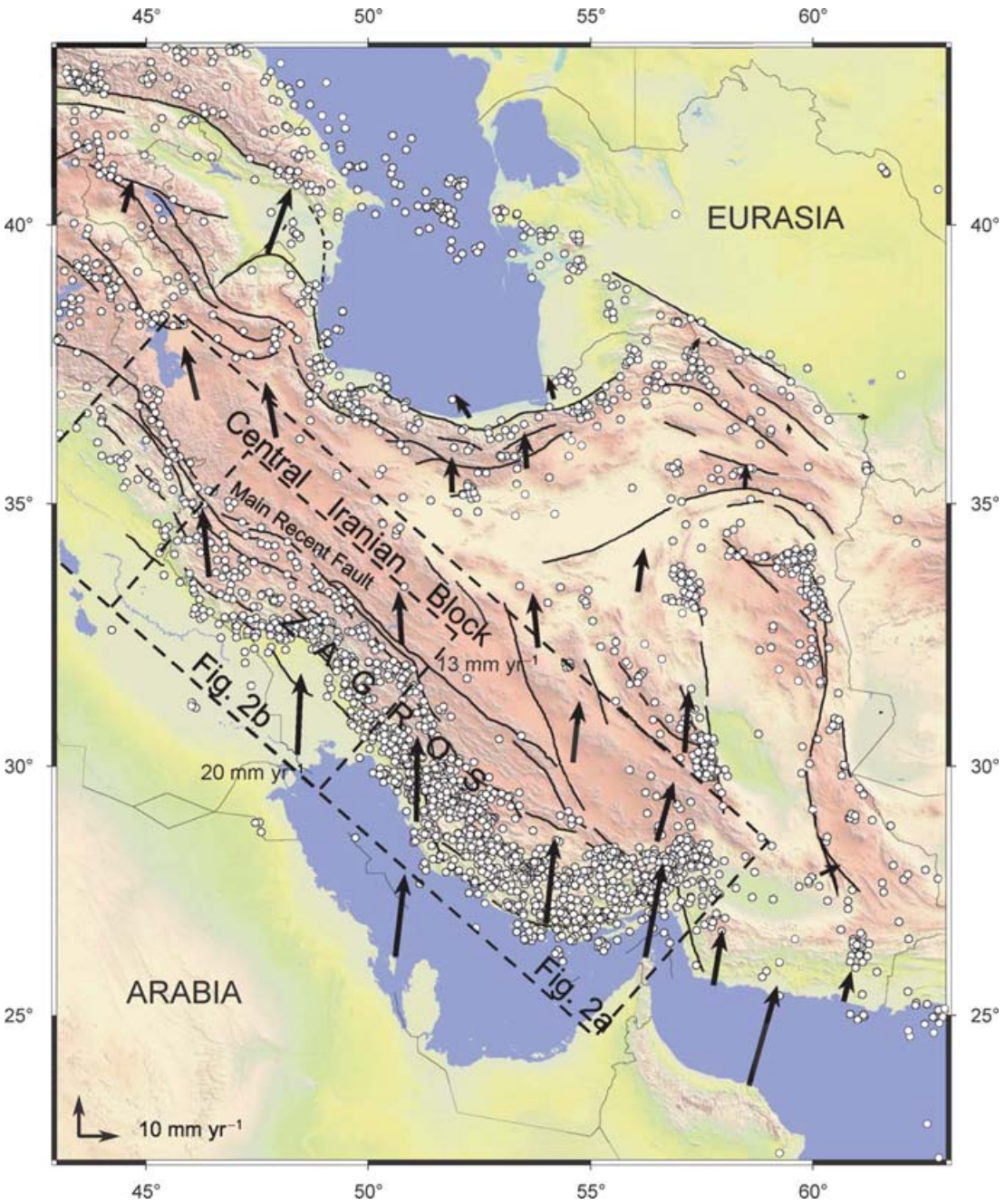

Figure 1. Framework of the Arabia-Eurasia collision in Iran. Circles show instrumental seismicity, arrows display the GPS velocity field as computed by Vernant *et al.* (2004), thick solid lines represent active faults, thin solid lines match political boundaries.

suture), the convergence direction occurs at 45° relative to the belt axis, the normal and parallel range velocities being 5 mm yr^{-1} on in a CIB reference frame (Fig. 2).

Distinct deformation modes have been proposed for the NW and SE Zagros which are separated by the Kazerun fault (Figs 1 and 2). The tectonic activity of NW Zagros is bounded to the NE by the main recent fault (MRF). Despite the millennial historical recording of earthquakes in Iran, no extensive sequence of large earthquakes is known along the MRF. However, its seismic character is assessed by the 1909 Silakhur earthquake (Ambraseys & Melville 1982). At a longer timescale, geomorphic studies of the MRF also point out its activity with various fault slip rates estimates : ∼6 mm yr^{-1} (O. Bellier, personal communication, 2005), 10–17 mm yr^{-1}. (Talebian & Jackson 2002; Bachmanov *et al.*, personal communication 2004). In the Zagros fold and thrust belt south to the MRF, most of the seismic deformation corresponds to thrusting events with slip vectors normal to the main structural trend. (Talebian & Jackson 2004). Therefore, these data may indicate that most of the parallel component of oblique convergence is taken by the MRF. However, the velocity of the MRF based on geological evidences is always higher than velocity estimated using geodetic measurements, which give an upper bound of 5 mm yr^{-1} (Vernant *et al.* 2004). Such discrepancy may come from the assumption made by (Talebian & Jackson 2002) that the MRF activity began 5 Ma ago, however, this assumption is not constrained by any data. Alternatively, recent reorganization of Iranian tectonics (Allen *et al.* 2003) implies that geodetic data do

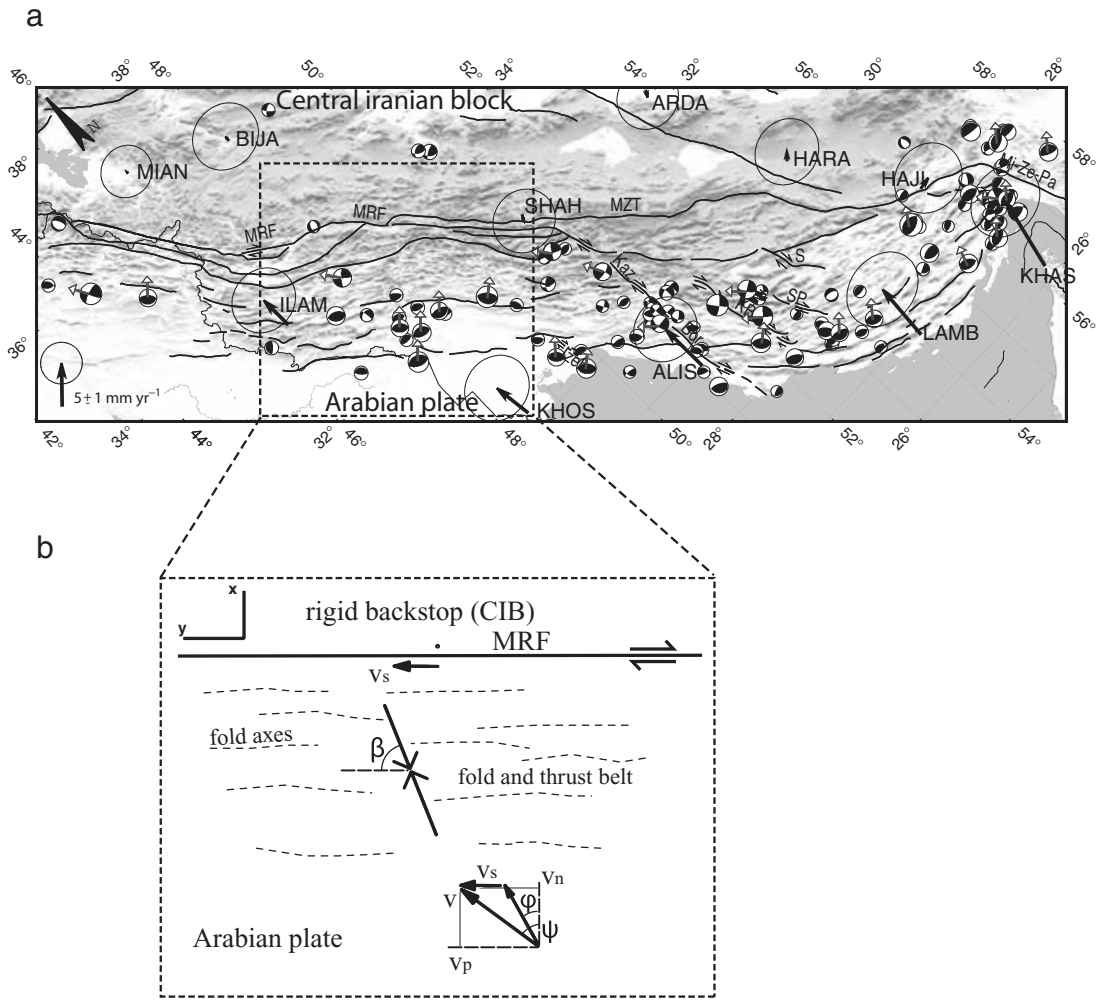

Figure 2. (a) Geodetic and seismologic features of the Zagros superimposed to a relief map. GPS velocity field is shown by arrows with respect to a fixed CIB (sites MIAN, BIJA, SHAH and ARDA on figure). Focal mechanisms and slip vectors are from Harvard CMT database (http://www.seismology.harvard.edu), slip vectors show the motion of the SW block. Solid lines display main faults (MRF: Main Recent Fault; MZT: Main Zagros Thrust; Kaz: Kazerun; Bor: Borajzan; KB: Kareh Bas; SP: Sabz-Pushan; S: Sarvestan; Mi-Ze-Pa: Minab-Zendan-Palami). (b) Simplified map view of the deformation zone of Zagros. v represents the velocity of Arabia with respect to fixed CIB, v_n and v_p being the normal and parallel components of v. Fault slip rate is given by v_s. Plate convergence azimuth is given by ψ. The orientation of the maximum horizontal stress σ_1 with respect to the direction parallel to the orogen (y) is given by the angle β.

not represent the long term motion of Iran. The tectonic activity of the SE Zagros is significantly different, probably due to the transfer of motion induced by the Kazerun fault (Berberian 1995). East of the Kazerun fault, the main tectonic feature bordering the Zagros to the NE is the Main Zagros Thrust (MZT), which shows neither seismic nor geodetic activity (Tatar *et al.* 2002). Instead, this last study indicates that the deformation is distributed across the fold and thrust belt, suggesting wrenching rather than partitioning.

In this paper we examine the relation between the deformation of the fold and thrust belt of Zagros and the slip rate of the fault in contact with the rigid backstop (Fig. 2). To do so, we explore the boundary conditions and the mechanical parameters that may influence the present-day Zagros deformation and the MRF activity. Previous models of oblique convergence were developed to study oblique subduction (McCaffrey 1992) or accretionary prisms (Platt 1993). They are not well designed to describe the strain field within a continental orogen. First, the Zagros deformation occurs with two modes of deformation. In the fold and thrust belt, the strain is distributed and occurs on numerous folds and faults. On the MRF, the strain is concentrated on a few single discontinuities. Second, the style of deformation varies largely with depth in continental orogens. While the upper crust of the Zagros mostly deforms by friction and faulting (Tatar *et al.* 2004), ductile strain probably occurs in the mountain root at greater depth at temperature higher than 350°C. For these two reasons, a temperature dependent viscoelastoplastic modelling of the oblique deformation of this orogen is appropriate. Therefore, the mechanical setting of our model is close to previous 2-D (plain strain, vertical cross-section) numerical modelling developed for intracontinental orogens (Chery *et al.* 1991; Beaumont & Fullsack 1994; Braun & Beaumont 1995).

In this paper we first present the mechanical assumptions and the numerical method, then we study the influence of two main parameters:

(1) the obliquity of convergence ψ ranging from to 0° (frontal) to 90° (strike slip) and

(2) the strength of the MRF as controlled by the effective friction angle of the fault. We also study the sensitivity of our model to

other controlling factors such as the lithospheric thermal field and the mantle rheology. We finally analyse our numerical results with respect to an analytical formulation of slip partitioning.

MECHANICAL MODELLING

Numerical method and constitutive laws

The basic goal of this study is to model the influence of assumed rock rheology and boundary conditions on a steady state (or geological) deformation. We neglect here strain and stress variation due to the seismic cycle. Indeed, the average seismic stress drop is ∼3 MPa (Hanks 1977), much smaller than the total tectonic stress that can reach ∼150 MPa at seismogenic depths (Byerlee 1978). We assume that the mechanical system is always at quasi-static equilibrium, corresponding to a perfect balance inside the continuum medium between the internal forces (or stress) and external forces (gravity forces and tractions imposed at the boundary conditions). We use a numerical model based on the finite element method (FEM) which requires the resolution of a discretized system formed by the momentum equation, the constitutive law of the medium and static and kinematic boundary conditions. Numerical issues concerning the method and the corresponding software ADELI can be found in a previous paper (Chéry *et al.* 2001) and are not described here. Three elementary constitutive laws are used. In the elastic domain we use a linear relation between the strain rate and the stress rate tensor. Values adapted to the continental crust are chosen for the Young's modulus (10^{11} Pa) and for the Poisson's ratio (0.25). At low pressure and temperature, the elastic domain is limited by the frictional limit of fractured rocks (Byerlee 1967, 1978). In order to reproduce the dependence between the differential stress and the mean stress, we use a Drucker-Prager model, which depends on the internal friction angle ϕ, the cohesion c and the dilatancy angle. The yield criterion can be described as follows (Leroy & Ortiz 1989):

$$f(\sigma) = J_2(\sigma) - \alpha\left[\overline{\sigma} + \frac{c}{\tan\phi}\right] < 0$$

$$J_2(\sigma) = \sqrt{\frac{3}{2}}\sqrt{dev\sigma : dev\sigma}$$

$$\alpha = \frac{6\sin\phi}{3 - \sin\phi}$$

$$\overline{\sigma} = -\frac{1}{3}tr(\sigma),$$

where σ is the stress tensor, $\overline{\sigma}$ is the mean stress, *dev* is the deviatoric part of a tensor, and the colon represents the contracted product. The dilatancy angle is set to zero, therefore, leading to a non-associated plastic flow (the plastic potentially is simply equal to J_2 (σ)). The equivalent behaviour of the upper crust is elastic with a frictional limit. At higher temperature the strain rate dependent 'power law' rheology is approximated by a linear Maxwell model of viscoelasticity in which the fluidity γ ($\mathrm{Pa}^{-1}\,\mathrm{s}^{-1}$) depends on the temperature T as follows:

$$\gamma = \gamma_0^{e-E/RT},$$

where γ_w is a material constant, E is the activation energy and R is the gas constant. Following the concept of stress envelop (Brace & Kohlstedt 1980) we choose among viscoelastic and elastic frictional behaviours with considering that the rheology with minimum deviatoric stress invariant $J_2(\sigma)$ dominates (Chéry *et al.* 2001). According to this dual behaviour, our rheological model naturally reflects parameter variations such as temperature, stress and strain rate.

Geometry and boundary conditions

Because of the obliquity variation of convergence with longitude and due to the internal complexity of the Zagros, a full 3-D model would be needed to accurately represent the tectonic complexity of Fig. 2. However, we use a simpler model design in order to provide a simpler interpretation of our deformation model. We adopt a 2-D structural model as a vertical cross-section (x-z plane) perpendicular to the belt trend (Fig. 3) as done for the first mechanical model of Zagros (Bird 1978). The structural trend corresponds to the y. The obliquity of convergence is given by the horizontal angle ψ between the velocity imposed to the moving plate (the Arabian margin) and the x-z plane. As no variation along y occurs, all stress and strain rate related to y-derivatives fall to zero. Given the crustal structure of the Zagros (Dehghani & Makris 1984; Ni & Barazangi 1986) we adopt an isostatically compensated structure at Moho level according to averaged surface topography. Moho depth gradually increases from 40 km on the Arabian margin to 60 km in the zone of elevated (2.5 km) topography. However, the Moho depth below the CIB and especially the Sanandaj-Sirjan zone is not clearly defined probably due to a complex geological history of the CIB and crustal overthrusting during Zagros orogeny (Kaviani 2004). In order to match the topographic data, we adopt a maximum Moho depth of 60 km below the high topographic area of the Zagros and Sanandaj-Sirjan area, then switching to 40 km depth for the backstop area.

Thermal field

Because of the temperature effect on crustal and mantle viscosity, the thermal field may critically influence the Zagros deformation. The heat flow values on the Arabian plate are relatively well known and close to 40 $\mathrm{mW\,m^{-2}}$ (Pollack *et al.* 1993). A lack of published borehole temperature data makes the heat flow impossible to know on the Zagros and Sanandaj-Sirjan areas. Because the CIB has been shown to be rigid compared to the surrounding orogens like Zagros and Alborz (Vernant *et al.* 2004), we make here the assumption that this rigidity is due to a cold thermal field in this area, according to the estimated relation between the thermal state and the tectonothermal age of the continental areas (Chapman & Furlong 1977). We adopt here a surface heat flow of 40 $\mathrm{mW\,m^{-2}}$ as for Arabia. The thermal field in Zagros is less trivial to define, as the heat crossing this mountain may be the result of at least two processes. First, the progressive crustal thickening increases the radiogenic production inside the belt, increasing temperature with respect to the same depth on the two margins. Second, the onset of the Arabian mantle subduction below the Zagros could cause a temperature decrease in the Zagros crust above. In order to capture the effect of these processes, we compute two steady state thermal models according to the present-day Zagros crustal structure. No radiogenic production is taken for the mantle, and a basal heat flow of 10 $\mathrm{mW\,m^{-2}}$ coming from the mantle is assumed, it corresponds to a shield type Moho heat flow (Pinet *et al.* 1991). We use radiogenic productions for upper and lower crust of 1.5 and 0.5 $\mu\mathrm{W\,m^{-3}}$ respectively, in order to fit the 40 $\mathrm{mW\,m^{-2}}$ of the Arabian plate. In the case where mantle subduction is assumed, the downwelling of the cold mantle

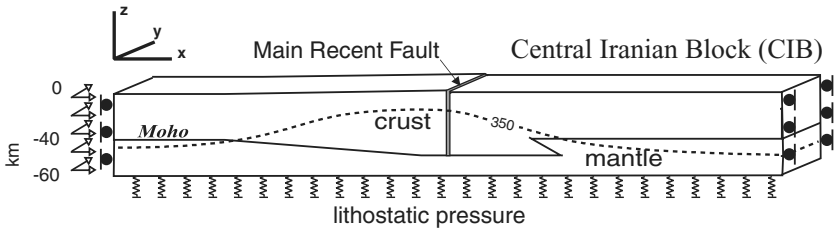

Figure 3. Block diagram of the 3-D mechanical model of Zagros. The right-hand side has fixed horizontal velocities, the left-hand side moves at a velocity v with normal and parallel components v_n (5 mm yr^{-1}) and v_p (5 mm yr^{-1}), respectively. Vertical boundaries have free slide velocities. The base of the model in the uppermost mantle is supported by hydrostatic pressure. The dashed line represents the 350°C isotherm.

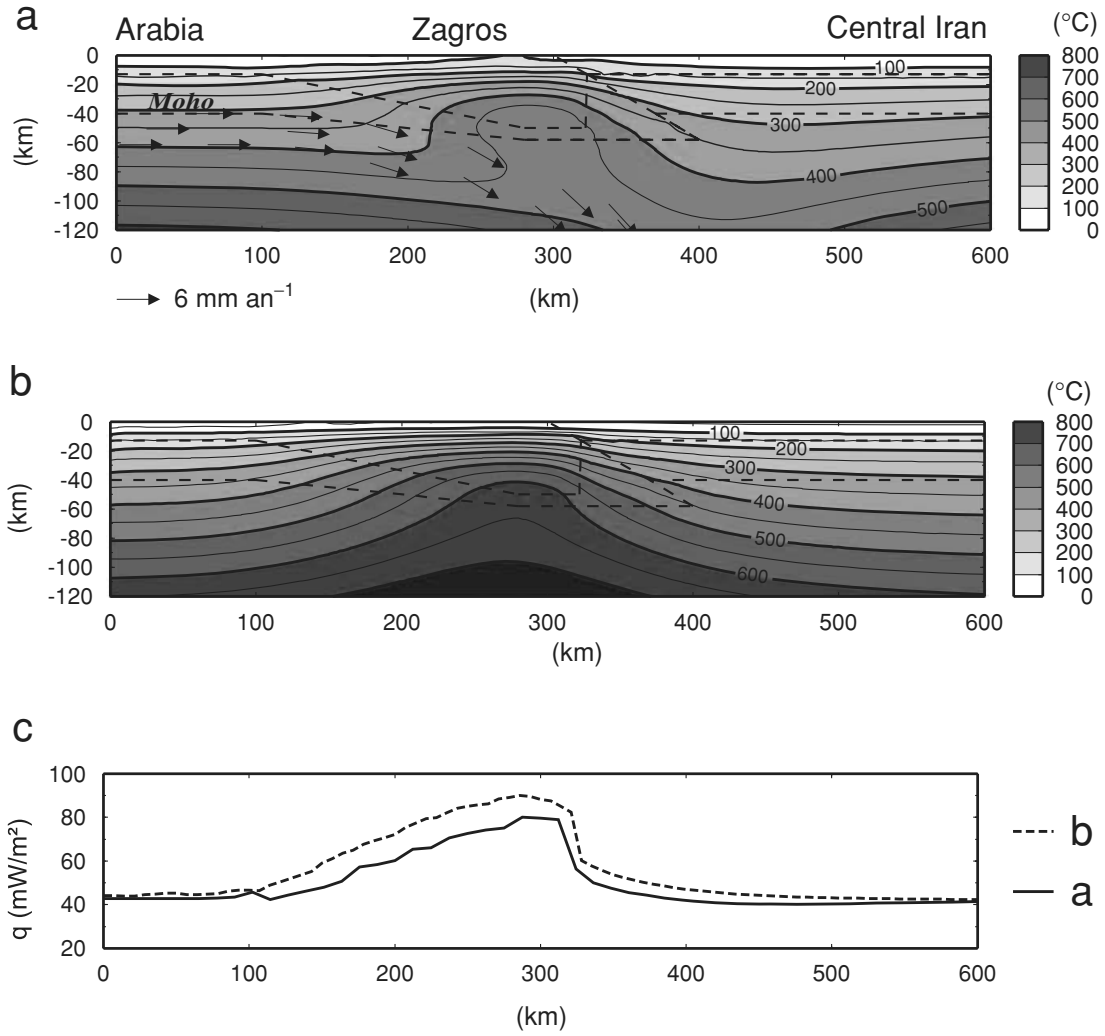

Figure 4. Thermal models used in the mechanical modelling. Dashed lines delimitate limits of the upper and lower crustal heat production (see table 1 for values). (a) Steady state temperature field associated to the Arabian mantle subduction (cold case). (b) Steady state temperature field without subduction (hot case). (c) Surface heat flow associated to the temperature fields above.

counteracts the heating due to crustal thickening (case referred as 'Cold'). Heat flow values increase up to 80 mW m^{-2} in the thickest part of the Zagros (Figs 4a and c). If no subduction takes place, meaning that mantle thickens rather homogeneously across the orogen, a larger heating occurs in the Zagros (case referred as 'Hot'), resulting in surface heat flow values 10 to 15 mW m^{-2} higher than for the former case (Figs 4b and c), and culminating to 90 mW m^{-2} in the vicinity of the MRF. Yet, these thermal predictions cannot be directly compared to data as no heat flow measurements are available for the Zagros. Based on the correlation between surface heat flow and seismicity depth in continental areas (Meissner & Strehlau 1982; Sibson 1982), these thermal fields appear compatible with a temperature of 350°C occurring between 10 and 20 km in Zagros. This depth range appears consistent with the maximum seismicity depth deduced from local seismic surveys in the SE Zagros (Tatar *et al.* 2004).

Table 1. Summary of physical parameters used in the thermal and mechanical modelling.

Name	Used symbol	Unit	Value
Cohesion	c	Pa	10^6
Friction angle	ϕ	°	3–7–15
Fluidity parameter	γ_0	$Pa^{-1}\,s^{-1}$	8.49 10^{-15} (crust) 4.8 10^{-19} (mantle)
Activation energy	E	$KJ\,mol^{-1}$	110 (crust) 83 (mantle)
Young's modulus		Pa	10^{11}
Poisson's ratio		–	0.25
Thermal conductivity		$W\,m^{-1}K^{-1}$	3
Mean specific heat		$J\,m^{-1}K^{-1}$	1000
Heat production (upper crust)		$\mu W\,m^{-3}$	1.5 (upper crust 0.5 (lower crust)

Rheological parameters

The chief aim of our numerical modelling is to investigate the effect of convergence obliquity on the internal deformation of the Zagros fold-and-thrust belt and of the slip rate of the MRF. To do so, we combined together the plane view depicted on Fig. 2(b) and the 'cold' thermal field of Fig. 4(a) to obtain the oblique convergence model of Fig. 3. The temperature field of the mechanical model comes from the thermal field experiments previously described. For the purpose of these experiments, we do not consider the temperature evolution with time. The mechanical model contains three rheological units: the crust, the uppermost mantle and the fault zone. Considering the relatively high mantle temperature obtained in the Zagros, we assume that the deep part of the lithosphere retains minor deviatoric stress. Therefore, we limit the model with a hydrostatic boundary condition at 60 km depth. Because this boundary condition is inside the mantle, no density contrast occurs here.

Constant elastic parameters adapted to the continental crust are chosen for the Young modulus (10^{11} Pa) and for the Poisson ratio (0.25). Also, a common feature of all the models tested is that the crust adjacent to the fault zone is strong, behaving as a frictional medium with a high coefficient of friction (0.6–0.8) and hydrostatic pore pressure (Townend & Zoback 2000). This rheological state is simulated with an internal friction angle of 15° for the Drucker-Prager model (Chéry *et al.* 2001). A quartz-like rheology is used for the viscous lower crust, assuming differential stress levels of ∼300 MPa at the brittle–ductile transition (Kohlstedt 1995). In order to fit this stress level and also to account for the stress decay with temperature, we calculate values for the parameters γ_0 and E to obtain a viscosity decay from 10^{23} Pa s at 350°C to a value of 10^{20} Pa s at 650°C. Our numerical model does not allow power law viscosity. Therefore, we use a 1-D strain rate–stress relation to make sure that the deviatoric stress magnitude we obtain with the linear approximation is consistent with a power law viscosity for a strain rate range of $[10^{-16}$–$10^{-15}\,s^{-1}]$.

Based upon laboratory-derived flow laws for olivine, the strength of the upper mantle has been viewed as strong for many years (Brace & Kohlstedt 1980). However, the maximum strength of the continental mantle is a subject of considerable uncertainty (Karato *et al.* 1986; Tsenn & Carter 1987). We, therefore, test models using olivine rheology corresponding to a strong mantle (Kirby 1983) (high strength in Table 2), models in which the mantle strength is limited to 600 MPa (medium strength in Table 2) and also using a weak mantle rheology (as weak as the crust, low strength in Table 2).

The rheology of active faults is largely unknown, but some geophysical evidences such as heat flow and stress measurements seem to indicate that effective friction of an active fault such as the San Andreas fault is low (Rice 1992). At ductile levels, some studies (Gueydan *et al.* 2003) suggest that localization processes due to deformation-aided phase transformation promote weaker strength in fault zones than in the protolith. We vary the fault strength using two effective fault friction angles corresponding to a low strength (3°) and to a moderate strength (7°) with respect to a high crustal strength (15°). Keeping in mind that the transposition of the

Table 2. Summary of input and output variables for all tested cases. Symbol meaning is given in the text and in figure captions.

Case N°	Thermal field	Mantle strength	MRF Friction (°)	Obliquity ψ(°)	v_s (mm yr^{-1})	v_s/v_p (per cent)	β(°)
1	Cold	Medium	3	0	0	–	90
2	Cold	Medium	3	22	0	0	78
3 (ref)	Cold	Medium	3	45	1.2	24	69
4	Cold	Medium	3	67	5.2	80	68
5	Cold	Medium	3	85	6.8	97	51
6	Cold	Medium	7	0	0	–	90
7	Cold	Medium	7	22	0	0	77
8	Cold	Medium	7	45	0	0	66
9	Cold	Medium	7	67	2.2	34	58
10	Cold	Medium	7	85	5.1	72	50
11	Cold	Low	3	45	1.3	26	70
12	Cold	High	3	45	0.9	18	69
13	Hot	Low	3	45	1.0	20	69
14	Hot	Medium	3	45	1.0	20	68
15	Hot	High	3	45	0.9	18	67

friction angle of the Drucker-Prager model into a Coulomb friction coefficient is depending on the principal stress values, these values of 3°, 7° and 15° corresponds approximately to Coulomb friction coefficients of 0.1, 0.3 and 0.6, respectively. The friction angle is the only parameter we change between the fault zone and the other part of the crust. Lowering the friction angle deepens the transition brittle/ductile, but below this transition zone the fault zone have the same properties as the surrounding crust.

Numerical experiments

In a first set of experiments we consider the variation of obliquity angle on a rheological model made with a cold thermal field (Fig. 4a), a medium mantle strength and a weak or medium MRF (Cases 1–10). In a second set of experiments (Cases 11–15) we specifically address the oblique convergence of Zagros (45° of obliquity) and study how thermal field, mantle strength variations may influence strain partitioning into the Zagros. In each of these experiments the time stepping is chosen in order to minimize the inertial forces. Only the results obtain when the experiments reach a steady state (i.e. the velocity value does not evolve anymore) are presented, this is usually achieve after a time corresponding to ∼3 Ma.

Reference case

We present the behaviour of a model corresponding to 45° obliquity convergence and to a low MRF strength (Case 3 or reference case). The deviatoric stress invariant $J_2(\sigma)$ of Fig. 5(a) displays three specific zones. From the surface to 20 km the deviatoric stress gradually increase from zero to 500 MPa. This effect is the direct consequence of the mean stress on the yield criterion. At greater depth in the lower crust, $J_2(\sigma)$ decays rapidly to values smaller than 100 MPa (in fact close to 1 MPa) due to strong temperature dependence. Because of the strain rate influence on the deviatoric stress, a given stress value in the lower crust does not coincide with a specific isotherm. In Arabia and in the CIB, the 400 MPa limit corresponds to 250°C, while a temperature of 300°C is reached under the Zagros. At greater depth in the uppermost mantle, stress ranges between 100 and 500 MPa, indicating that the mechanical lithosphere should be thicker than 60 km. We, therefore, perform a numerical experiment with setting the depth of the bottom hydrostatic boundary condition to 120 km. Because this experiment leads to identical results in term of crustal stress and strain than the model shown here, we consider our 60-km-thick model as reliable. Therefore, the stress distribution for our model corresponds to a strong upper crust partly coupled to the mantle in cold areas (Arabia and CIB). By contrast, decoupling between the upper crust and the mantle occurs in Zagros due to a low viscosity zone into the lower crust corresponding to temperature of 350–500°C.

The strain rate pattern of Fig. 5(b) displays a very different aspect from the stress pattern. The strain rate is layered vertically with a high strain rate occurring in the MRF and a diffuse zone of strain inside the Zagros orogen. Despite the strong stress variation with depth inside the crust, the strain rate does not vary much, suggesting that the crust deforms as a whole. According to the strain rate, the v_x velocity pattern does not vary inside Arabia, decaying only while crossing the Zagros. Upward pointing vectors near the surface and

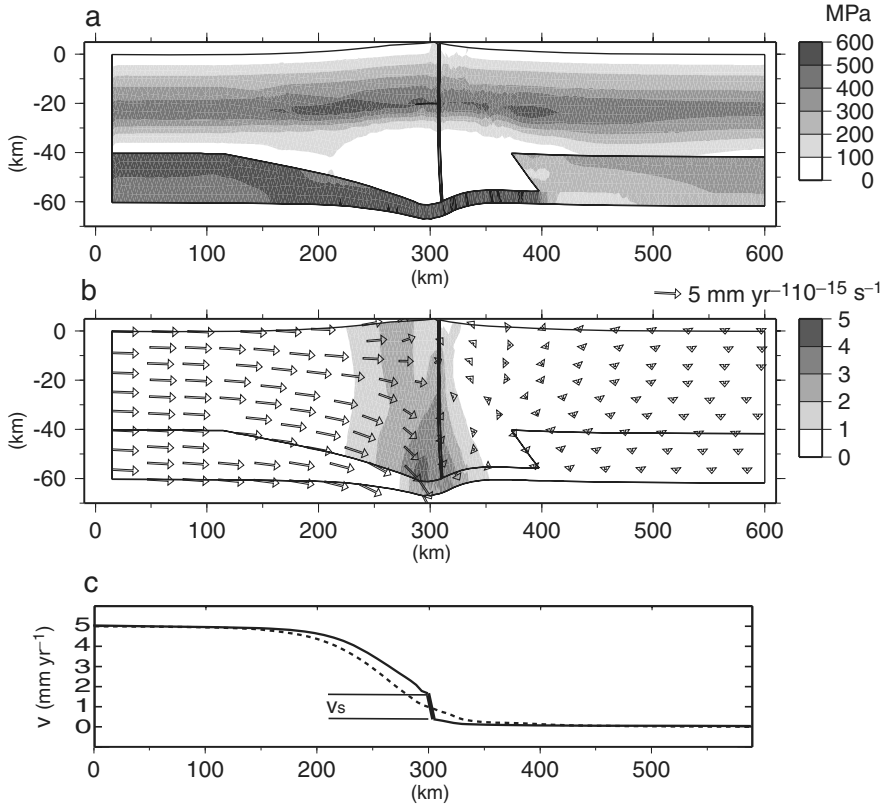

Figure 5. (a) Deviatoric stress field obtained after 3 Myr (∼15 km of shortening), showing high stress in the upper crust and the uppermost mantle, and a decoupling zone of low stress in the thick Zagros lower crust. (b) Velocity field and second invariant of the strain rate. (c) Parallel (solid line) and normal (dashed line) components of the surface velocity field. The large velocity gradient at $x = 300$ km corresponds to the differential velocity v_s across the Main Recent fault.

downward pointing vectors in the lower crust indicate that crustal thickening occurs at a maximum rate of 3 mm yr^{-1}. At greater depth the velocity pattern in the mantle suggests mantle subduction rather than homogeneous thickening. The evolution of surface velocity v_y along x-direction is roughly similar to the one of v_x (Fig. 5c), with constant velocity within the Arabian plate and the CIB. A moderate velocity gradient occurs in the Zagros, while a strong velocity gradient occurs when crossing the MRF. Therefore, the velocity pattern shows that only a part of the transcurrent deformation is taken by the MRF (1.2 mm yr^{-1}), this implies a significant wrenching (3.8 mm yr^{-1}) in the Zagros belt.

Obliquity effect

Keeping the modulus of velocity constant (7 mm yr^{-1}) we test obliquity angle ψ with values of 0, 22, 45, 67, 85°, with low and medium fault strength. Because strain and stress invariants are a blend of all tensor components, and also due to the strong control of mean stress and temperature, all cases listed in Table 2 present stress and strain patterns similar to the ones shown for case 3 (Figs 5a and b). However, significant kinematic changes occur on the strike-slip velocity of the MRF (v_s). These variations are expressed in Table 2 in term of absolute slip rate (v_s) and normalized slip rate (v_s/v_p), v_p being the range parallel component. Zero obliquity (i.e. frontal convergence, cases 1 and 6) is a trivial case as it means that $v_s = v_p = 0$. When $\psi = 22°$, the MRF remains inactive (cases 2 and 7), meaning that all the shear deformation occurs in the Zagros. The case with $\psi = 45°$ and a weak MRF corresponds to the reference case 3. Only 24 per cent of the y-velocity occurs on the fault. If a medium strength fault is used (case 8), the MRF remains inactive. Only for large obliquity angles (67 and 85°, cases 9 and 10) the fault motion occurs with a medium MRF fault friction, with 34 and 72 per cent of the y-velocity taken by the fault. A low strength fault and a large obliquity angle is the only situation where almost all the y-velocity occurs on the fault (80 per cent and 97 per cent, for cases 4 and 5, respectively).

The normalized fault slip rates for cases 1–10 are summarized in Fig. 6. Also, we compute the angle β of the direction of the maximum compressive stress σ_1 direction within the Zagros with respect to the fault azimuth. By contrast to the slip rates, the evolution of β is almost linear with obliquity angle and similar for the low friction and medium friction cases.

Thermal and mantle strength variations

Starting from the reference case 3, which corresponds to a weak MRF and a 45° obliquity angle, we now vary the rheological properties of the uppermost mantle (high strength mantle, low strength mantle with viscoelastic parameters equal to those of the crust). We use also a hot thermal field corresponding to homogeneous hypothesis for the Zagros deformation (hot case, Fig. 3b). All these variations, summarized in the Table 2 (cases 11–15) lead to minor deviation of slip rates with respect to case 3, it shows that the lower crust is effectively decoupling the upper crust from the mantle. Fault velocity v_s ranges from 0.9 to 1.3 mm yr^{-1} (18–26 per cent). The angle for maximum compression varies less with values ranging from 67° to 69°. Therefore, key factors controlling the Zagros internal deformation and MRF slip rate seem to be the obliquity angle and the MRF strength. In the following we first attempt to compare our modelling results to geologic and geodetic data in the SE and north Zagros. We then propose an explanatory model for the strain pattern suggested by our numerical experiments.

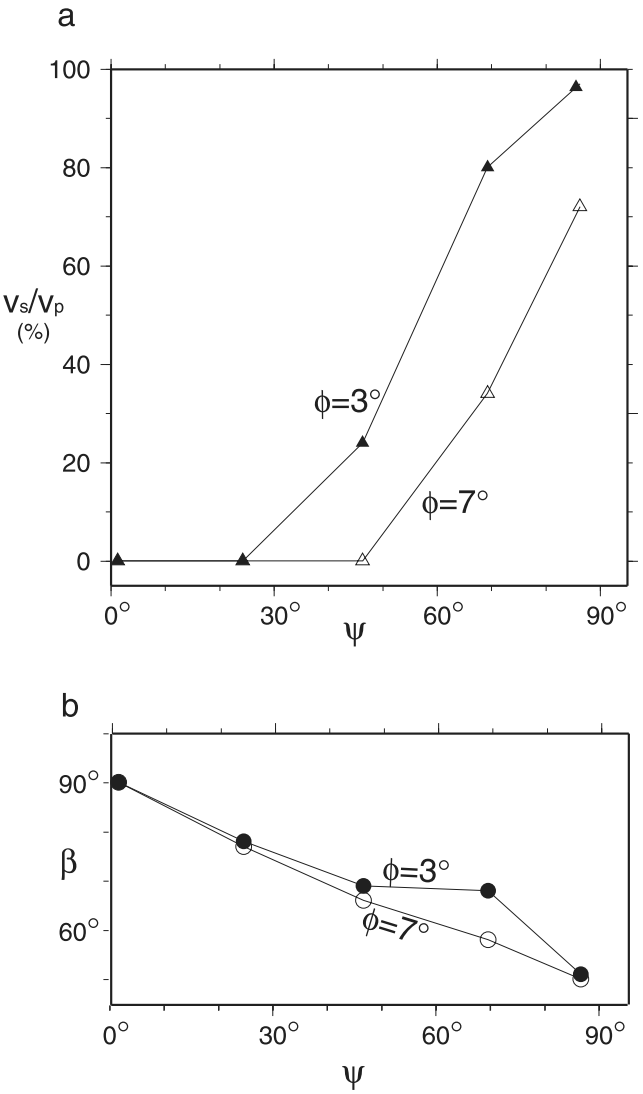

Figure 6. (a) Fault slip rate normalized to the parallel motion with respect to plate obliquity ψ and effective fault friction ϕ gor cases given in Table 2. Solid triangles refer to $\phi = 3°$ and empty triangles refer to $\phi = 7°$. Low obliquities (<25°) correspond to inactive strike-slip faulting. (b) Corresponding maximum horizontal strain orientation in the Zagros ($x = 270$ km) are given by solid ($\phi = 3°$) and empty ($\phi = 7°$) circles. The cause of the departure from linearity at $\psi = 70°$ for $\phi = 3°$ is not known and would require more numerical experiments.

DISCUSSION

Earthquakes and strain in Zagros

Based on GPS geodesy, the motion of NW Zagros occurs with an obliquity of 45° ± 5° with respect to the CIB. Therefore, our numerical model predicts that the slip rate of a weak MRF could reach only 26 per cent of the full orogen-parallel velocity, that is, 1.3 mm yr^{-1} as the differential velocity between the CIB and the Arabian plate is ∼7 mm yr^{-1}. Geodetic, geologic and seismologic information about the motion of the MRF are required in order to check our

model validity. Recently, a local GPS network has been installed in NW Zagros (within dashed rectangle in Fig. 2) in order to document the interseismic velocity field. These results are still preliminary due to the short interval between the two surveys (2 yr). At some distance (∼50 km) to the fault trace where the interseismic velocity should match the geological fault slip rate, no large variation of the range parallel velocity is occurring in the MRF vicinity near 34° of latitude (Hessami *et al.* 2006, Walperdorf, oral communication). Therefore, it is unlikely that this fault could absorb all the tangential motion between the Arabian plate and the CIB. On the other hand, geomorphic features of strike-slip faulting have clearly been documented for the MRF (Talebian & Jackson 2002; Bachmanov *et al.* 2004), even if no slip rate constrained by geochronological dating has been published to date. A partitioning model has been proposed in the NW Zagros on the base of earthquake focal mechanisms analysis (Talebian & Jackson 2004). A large number of the focal mechanisms in the NW Zagros suggests reverse faulting. Moreover, the strikes are subparallel to local trends of topography and fold axes. Therefore, these authors propose that oblique shortening is partitioned into right-lateral strike-slip on the MRF and orthogonal shortening within the Zagros fold and thrust belt. This proposition is not consistent with our numerical model results, except if we use an effective friction angle lower than 3° (which corresponds to an equivalent friction coefficient of 0.05). A key test for partitioning hypothesis in NW Zagros is the orientation of shortening axes inside the fold and thrust belt. Most of the focal mechanisms displays slip vectors normal to the overall belt trend (Talebian and Jackson 2002, 2004). However, a recent quantitative analysis of geodetic and seismic strain (Masson *et al.* 2005) brings two results of interest for our discussion. First, the seismic and geodetic strain directions are consistent, but the seismic to geodetic strain ratio in the Zagros is very low (5 per cent), suggesting that most of the strain occurs aseismically, as suggested by the pioneering work of (Jackson & McKenzie 1984). Therefore, it could be possible that some wrenching deformation occurs in an aseismic way in the Zagros. Second, (Masson *et al.* 2005) computed also the seismic strain rate tensor within Iran using the Kostrov's moment tensor summation. They found a similar direction (14°–18° N) for the maximum compressive strain orientation within the NW and SE Zagros. The geodetic strain tensors are computed using sites free from any interseismic effects. Therefore, seismic and geodetic strain directions seem to be representative of the long term strain tensor. As the NW Zagros and the MRF strikes at N 135°E, and assuming that strain rate tensors and stress tensor have coincident principal axes, this leads to a maximum compressive stress σ_1 direction within the Zagros of 59°–63° with respect to the fault azimuth. Clearly, this direction is more compatible with modelled values (67–70°) given by our experiments than with the normal direction (90°) corresponding to a full partitioning hypothesis. Because the values found by Masson *et al.* are significantly different from Talebian and Jackson results, further studies are needed to better assess the seismic strain regime in Zagros.

The SE Zagros east to the Kazerun fault is a more complicated example of oblique convergence. Indeed, the Zagros fold axes direction becomes progressively E–W, and the fault system appears as a mix of thrusts interconnected with active strike-slip faults which accommodate some of the range parallel motion (Fig. 2, (Tatar *et al.* 2004). Nevertheless, it remains clear that the obliquity angle is smaller than for the NW Zagros, ranging between 10° and 30°. No strike-slip faulting occurs along the northern border of the Zagros, indicating that most of the oblique convergence is accommodated by the fold and thrust belt. This behaviour appears compatible with our mechanical model which predicts that a vertical fault should be inactive with obliquities ranging between 10° and 30°.

Strike-slip fault activity in obliquely convergent zones

Our model predicts that a strike-slip fault similar to the MRF in Zagros becomes active when the obliquity angle ψ exceeds 25–45° (depending on the fault friction). Here, we attempt to link this prediction to the mechanics of oblique convergence. Previous studies of oblique convergence mechanics rely mainly on two distinct hypotheses. In one approach, the lithosphere is rigid, and the motion is accommodated by a dipping fault and a vertical fault (Fitch 1972; Jones & Wesnousky 1992; McCaffrey 1992; McCaffrey *et al.* 2000; Bowman *et al.* 2003). This view seems appropriate to describe oblique subduction or continental faulting. It is questionable to decide if this approach is appropriate to describe the Zagros kinematics. Indeed, the Zagros mountain building may correspond to the accumulation of medium intensity earthquakes and aseismic deformation spread across a wide zone of 150 km in SE Zagros (Tatar *et al.* 2004). The sum of all deformation processes (including large earthquakes) over geological timescale results in a finite shortening of ∼50 km distributed among the fold and thrust belt (Blanc *et al.* 2003). Another geophysical finding is that most of the recorded fault dip ranges 30°–60°, ruling out the possibility that earthquakes occur on a seismically active low angle thrust (Talebian & Jackson 2004). If we assume that the lower seismicity limit corresponds to the onset of ductile deformation (Sibson 1982), the mechanical state of the Zagros should correspond to a strong upper crust floating over a weak lower crust, which decouples the upper crust from the mantle. We mean here that due to low shear stress on horizontal plane in the lower crust (i.e. the stress component $\sigma_{xz} < 20$ MPa), the mantle cannot drive the crust by basal coupling. In our experiment, the same far field velocity is applied to the crust and the mantle along the southern boundary (it corresponds to the Arabian plate velocity). Due to this setting, we argue that the mantle is mechanically decoupled from the crust, without being kinematically independent. Therefore, a plausible Zagros stress model should be similar to the Fig. 5a, that is, a stress guide of about 15 km in the upper crust and a vertical shear zone corresponding to the MRF. In this view, an alternative model for the Zagros strain may consider that the motion parallel to the structure is accommodated by bulk deformation of the lithosphere (wrenching) and possibly by a vertical fault as proposed for many orogens (e.g. San Andreas fault system) or frontal forearc regions (Platt 1993; Ellis *et al.* 1995; Krantz 1995; Teyssier & Tikoff 1998; Tikoff & Peterson 1998).

A discussion about the prevailing deformation mode of Zagros (discontinuous or continuous) is beyond the scope of our paper. In the following, we take for purpose of reasoning the McCaffrey's approach, assuming that crustal strain occurs on dipping planes in the high stress upper crust and on vertical planes in a low stress shear. Force balance considerations can then be written (McCaffrey 1992). The total horizontal shear force on the vertical strike-slip fault is $F_s = Z_s \tau_s$, where Z_s is the fault width and τ_s the average shear stress on the fault. This force is parallel to the y of Fig. 2(b). The total shear force on the thrust fault is $F_t = Z_t \tau_t / \sin\delta$, where Z_t is the fault depth, τ_t is the average shear stress and δ is the dip of the thrust fault. The horizontal shear force parallel to y is $F_y = Z_t \tau_t \sin\varphi / \sin\delta$, where φ is the horizontal angle of the thrust slip vector (see Fig. 2b). The admissible values of φ ranges between 0 and ψ. Because $F_y = F_s$, this requires $Z_s \tau_s = Z_t \tau_t \sin\varphi / \sin\delta$. Assuming

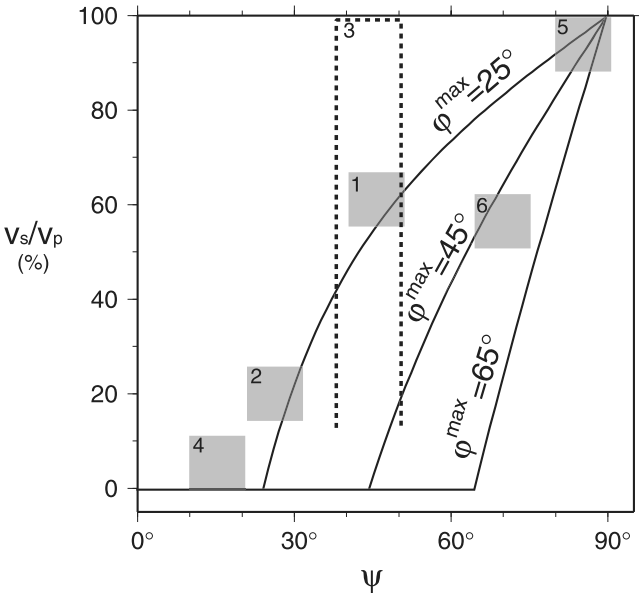

Figure 7. Fault slip rate normalized to parallel motion (v_s/v_p) with respect to plate obliquity ψ for three values 25°, 45° and 65° of the limit angle $\varphi^{\max}$ following the model of McCaffrey. Squared boxes represent the position of the normalized slip rate versus local convergence obliquity for the zones cited in the text (1 = west Great Sumatra fault; 2 = east Great Sumatra fault; 3 = Main Recent fault; 4 = SE Zagros; 5 = Central San Andreas fault; 6 = San Andreas fault in the big bend area).

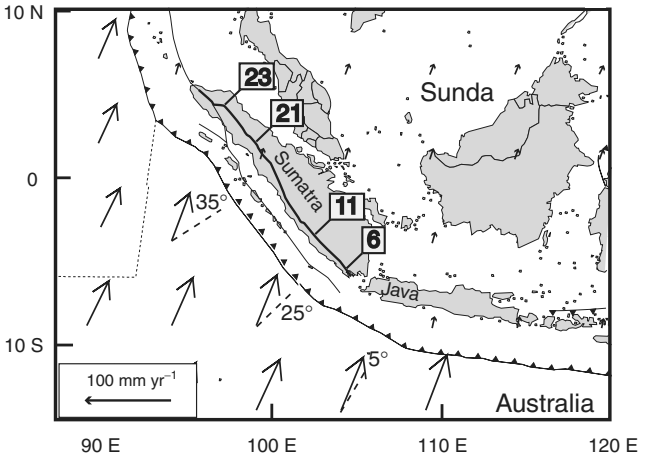

Figure 8. Oblique convergence between Australian and Sunda plates in Sumatra and slip rate of of the Great Sumatra fault (heavy line), adapted from Baroux *et al.* 1998. Velocities are given with respect to Eurasia. Slip rate of the Great Sumatra fault is large in northwest Sumatra where the convergence is oblique and rapidly decreases towards the southeast where convergence is more frontal. Geological slip rates along the fault are given by boxed numbers in mm yr^{-1}. Strike-slip motion ceases approximately in the Sunda strait between Sumatra and Java.

that the thrust faults within the fold and thrust belt and the MRF are in a similar tectonic environment we assume for the purpose of reasoning that $Z_s = Z_t$, implying that $\tau_s = \tau_t \sin\varphi/\sin\delta$. If we assume that the strike-slip fault can slip when τ_s reaches its maximum value $\tau_s^{\max}$, two cases may occur. At low ψ, the maximum value $\tau_s^{\max}$ cannot be reached. The strike-slip fault is locked ($v_s = 0$), implying that all the plate motion is taken by oblique slip on the thrust fault ($\varphi = \psi$). At high ψ, the maximum value $\tau_s^{\max}$ is reached, implying that φ cannot overcome a limit value $\varphi^{\max}$ equal to $\arcsin(\sin\delta \cdot \tau_s^{\max}/\tau_t)$. Looking back to Fig. 2(b), it is clear that equating $\varphi^{\max}$ to φ leads to $v_p = v_n \cdot tg\psi$ and $v_p - v_s = v_n \cdot tg\varphi^{\max}$. In this case, the vertical fault slips at a rate $v_s/v_p = 1 - \frac{tg\varphi^{\max}}{tg\psi}$. Despite its simplicity, this analysis predicts a slip rate evolution (Fig. 7) similar to what we found using our numerical model (Fig. 6). McCaffrey's model has been mainly used to understand the mechanics of oblique subduction zones. One of the best studied areas is the Sumatra subduction zone and the great Sumatra strike slip-fault (Fig. 8). Strike-slip faulting in the Sumatra-Java arc is very clear in northern Sumatra Island ($v_s \sim 20$ mm yr^{-1}) but decreases in southern Sumatra Island ($v_s \sim 6$ mm yr^{-1}) and seems to be elusive in Java Island where obliquity is near frontal (Baroux *et al.* 1998). If we assume that northern Sumatra corresponds to $v_s/v_p \sim 0.66$, $\psi \sim 50°$, $\delta \sim 30°$ (McCaffrey *et al.* 2000), it is therefore possible to predict that $tg\varphi^{\max} = 0.33 \cdot tg50$, that is, $\varphi^{\max} = 21°$. This set of values also imply that $\tau_s/\tau_t = \sin\varphi^{\max}/\sin\delta = 0.7$. It is interesting to notice that the limit obliquity of 21° seems consistent with the inactivity of the great Sumatra fault east of the Sunda strait. The prediction of shear stress ratio between the thrust and the strike-slip fault is difficult to compare to geophysical data, as direct stress measurements do not exist in this area. However, if one believes that the Sumatra-Java subduction interface has weak effective friction (as often proposed for the mechanical behaviour of subduction zones), then the great Sumatra fault would be still weaker.

The analysis we have done may also be compared to the results of Braun & Beaumont (1995) that modelled oblique convergence using a similar mechanical formulation in term of constitutive laws and lateral boundary conditions. The main difference between these two models is that they forced the crustal deformation by the subduction of the lithospheric mantle. As a result, the strain localization occurs in the zone where mantle detach to the crust. Despite the Braun and Beaumont model's has a different treatment of boundary condition, it also produces markedly different strain pattern according to convergence obliquity. At large obliquity (almost parallel motion) two sets of structures develop and the strain is partitioned. This behaviour is found in our model for values of ψ larger than 60°. At more frontal convergence, the Braun and Beaumont model's produces a single dipping shear zone. This kind of strain is likely to occur in our Zagros model when ψ is smaller than 30°, leaving the vertical fault inactive.

Due to the lack of data concerning the MRF slip rate, this analysis concerning the limit obliquity cannot be performed for the Zagros. The only firm knowledge we have is that the MRF is active in the NW Zagros where $\psi \sim 45°$, but not in the SE Zagros where $\psi < 20°$, meaning that $20° < \varphi^{\max} < 45°$. Both our model and the McCaffrey's model predicts that a complete partitioning between a pure thrust fault and a strike-slip fault is difficult to achieve when $\psi = 45°$. According to these models, the MRF in the NW Zagros should not display a slip rate larger than 2 or 3 mm yr^{-1}. Also, our model predicts an inactive MRF if the fault is moderately weak. Because the MRF is clearly active, this would mean that the MRF behaves as a weak fault. More generally, a fully partitioned model between a pure thrust fault and a strike-slip fault should occur only if obliquity is larger than 70°–80°. In this respect, the San Andreas Fault system may be used as a test for this prediction. The central San Andreas Fault system presents normal and tangential velocities of 3 and 34 mm yr^{-1}, respectively, ($\psi = 85°$). There the SAF slip rate is 34 mm yr^{-1}, absorbing the whole tangential velocity, meaning the oblique convergence is partitioned between a pure thrust and strike-slip fault (Mount & Suppe 1987; Jones & Wesnousky 1992). In the Big Bend area 200 km to the South, the obliquity decreases to

70°, and the SAF slip rate is only 18 mm yr^{-1} (Thatcher 1990), implying that ∼55 per cent of the tangential velocity is accommodated off to the SAF. Therefore, obliquity in convergent zones seems to be an important parameter which controls the slip rate of the strike slip faults and by the way the strain partitioning within the collision zone.

CONCLUSIONS

This 3-D mechanical modelling of the Zagros emphasizes that fault friction and obliquity of convergence are two important factors controlling the partition of deformation between an internally deformable fold and thrust belt and a vertical strike-slip fault. However, the obliquity of convergence is the most important parameter since low obliquity of convergence [0–25°] leads the vertical fault to be inactive if the effective friction angle is higher than 3°. However, it can be expected that a still lower friction would allow to keep the vertical fault active. Therefore, we propose that the SE Zagros does not correspond to this case, explaining why no right-lateral shear occurs in the main Zagros thrust vicinity. Intermediate obliquity [45°] similar to the one occurring in the NW Zagros does not lead the strike-slip fault to accommodate more than 26 per cent of the total lateral shear strain. The remaining shear strain could either occur in the orogen itself by a more distributed deformation, or by oblique slip on the thrust faults. Based on focal mechanisms, oblique slip on the thrust faults within the NW Zagros folds and thrusts belt can be rule out, and a full partitioning (with the MRF accommodating all the strike slip component between the Arabian plate and the CIB) suggested (Talebian & Jackson 2004). However, the recent results of a GPS study in the NW Zagros do not seem to support a full partitioning (Hessami *et al.* 2006) and in this way support our model. The GPS results are preliminary since they are based on two campaigns spaced by two years, and the seismicity (Hessami *et al.* 2006) may suffer from a too short interval of time recording, but comparing the two could lead to a better understanding of the active deformation in the Zagros. If the slip rate of the MRF is about 25 per cent of the overall strike slip motion between Arabia and the CIB, and if seismicity within the fold and thrust belt occurs only on the thrust faults then two question arise: first where are the structures which accommodate the other 75 per cent of the overall range parallel motion, and second what are the mechanisms involved? Further seismological and geodetic investigation need to be done to fully understand the mechanisms of the Zagros deformation. However, our simple analytical model can be used to estimate the strain partitioning in oblique collision zones based on the obliquity of the convergence.

ACKNOWLEDGMENTS

We thank Christophe Vigny and Olivier Bellier who shared interesting information on the partitioning and fault activity on the Sumatra Island. The manuscript has largely been improved by contructive and detailed comments from Susan Ellis and an anonymous reviewer.

REFERENCES

Allen, M.B., M.R. Ghassemi, M. Sharabi & Qorashi, M., 2003. Accomodation of late Cenozoic oblique shortening in the Alborz range, Iran. *J. Struct. Geol.,* **25,** 659–672.

Ambraseys, N.N. & Melville, C.P., 1982. *A History of Persian Earthquakes*. Cambridge University Press, New York.

Bachmanov, D.M., Trifonov, V.G., Hessami, K., Kozhurin, A.I., Ivanova, T.P., Rogozhin, E.A., Hademi, M.C. & Jamali, F.H., 2004. Active faults in the Zagros and central Iran. *Tectonophysics,* **380,** 221–241.

Baroux, E., Avouac, J.P., Bellier, O. & Sébrier, M., 1998. Slip-partitioning and fore-arc deformation at the Sunda trench, Indonesia. *Terra Nova,* **10,** 139–144.

Beaumont, C.P. & Fullsack, H.J., 1994. Styles of crustal deformation in compressional orogens caused by subduction of the underlying lithosphere. *Tectonophysics,* **232,** 119–132.

Berberian, M., 1995. Master blind thrust faults hidden under the Zagros folds: active basement tectonics and surface morphotectonics. *Tectonophysics,* **241,** 193–224.

Bird, P., 1978. Finite element modeling of the lithospheric deformation: the Zagros collision orogeny. *Tectonophysics,* **50,** 307–336.

Blanc, E.J.-P., Allen, M.B., Inger, S. & Hassani, H., 2003. Structural styles in the Zagros simple Folded zone, Iran. *J. Geol. Soc. London,* **160,** 401–412.

Bowman, D., King, G. & Tapponier, P., 2003. Slip partitioning by elastoplastic propagation of oblique slip at depth. *Science,* **300,** 1121–1123.

Brace, W.F. & Kohlstedt, D.L., 1980. Limits on lithospheric stress imposed by laboratory experiments. *J. Geophys. Res.,* **85,** 6248–6252.

Braun, J. & Beaumont, C., 1995. Three-dimensional numerical experiments of strain partitioning at oblique plate boundaries: Implications for contrasting tectonic styles in the southern Coast Ranges, California, and Central South Island, New Zealand. *J. Geophys. Res.,* **100,** 18 059–18 074.

Byerlee, J.D., 1967. Frictional characteristics of granite under high confining pressure. *J. Geophys. Res.,* **72,** 3639–3648.

Byerlee, J.D., 1978. Friction of rocks. *Pure and applied Geophysics,* **116,** 615–626.

Chapman, D.S. & Furlong, K.P., 1977. Continental heat flow-age relationship. *EOS Trans. Am. Geophys. Union,* **58,** 1240.

Chery, J., Vilotte, J.P. & Daignieres, M., 1991. Thermomechanical model of a thinned continental lithosphere under compression: implications for the Pyrenees. *J. Geophys. Res.* **96,** 4385–4412.

Chéry, J., Zoback, M.D. & Hassani, R., 2001. An integrated mechanical model of the San Andreas Fault in central and northern California. *Journal of Geophysical Research,* **106**(B10): 22 051–22 066.

Dehghani, G.A. & Makris, J., 1984. The gravity field and crustal structure of Iran. *N. Jb. Geol. Paläont. Abh.,* **168,** 215–229.

Ellis, S., Fullsack, P. & Beaumont, C., 1995. Oblique convergence of the crust driven by basal forcing: implications for length-scales of deformation and strain partitioning of orogens. *Geophys. J. Int.,* **120,** 24–44.

Fitch, T.J., 1972. Plate convergence, transcurrent faults and internal deformation adjacent to southeast Asia and the western Pacific. *J. geophys. Res.,* **77,** 4432–4460.

Gueydan, F., Leroy, Y., Jolivet, L. & Agard, P., 2003. Analysis of continental midcrustal strain localization induced by microfracturing and reaction-softening. *J. geophys. Res.,* **108,** NIL_80–NIL_97.

Hanks, T., 1977. Earthquake stress drop, ambient tectonic stress, and stress that drive plate motions. *Pageoph,* **115,** 441–458.

Hessami, K., Nilforoushan, F. & Talbot, C.J., 2006. Active deformation within the Zagros mountains deduced from GPS measurements. *J. Geol. Soc. London,* **163,** 143–148.

Jackson, J. & McKenzie, D., 1984. Active tectonics of the Alpine-Himalayan belt between Turkey and Pakistan. *Geophysical Journal of the Royal Astronomical Society,* **77,** 185–264.

Jones, C.H. & Wesnousky, S.G., 1992. Variations in Strength and Slip Rate Along the San Andreas Fault System. *Science,* **256,** 83–86.

Karato, S.H., Paterson, M.S. & Fitzgerald, J.D., 1986. Rheology of synthetic olivine agregates: influence of grain size and water. *J. geophys. Res.,* **91,** 8151–8176.

Kaviani, A., 2004. La chaıne de collision continentale du Zagros (Iran) : structure lithosphérique par analyse de données sismologiques. *Observatoire des Sciences de l'Univers de Grenoble*. Grenoble, Université Joseph Fourier: 228.

Kirby, S., 1983. Rheology of the lithosphere. *Reviews of Geophysics and Space Physics,* **21,** 1458–1487.

Kohlstedt, D.L., 1995. Strength of the lithosphere: constraints imposed by laboratory experiments. *Journal of Geophysical Research,* **100,** 17 587–17 602.

Krantz, R.W., 1995. The transpressional strain model applied to strike-slip, oblique-convergent and oblique-divergent deformation. *J. Struct. Geol.,* **17,** 1125–1137.

Leroy, Y. & Ortiz, M., 1989. Finite element analysis of strain localization in frictional materials. *Int.J. Numer. Anal. Methods Geomech.,* **13,** 53–74.

Masson, F., Chéry, J., Hatzfeld, D., Martinod, J., Vernant, P., Tavakoli, F. & Ghafori-Ashtiany, M., 2005. Seismic versus aseismic deformation in Iran inferred from earthquakes and geodetic data. *Geophys. J. Int.,* **160,** 217–226.

McCaffrey, R., 1992. Oblique plate convergence, slip vectors, and forearc deformation. *J. Geophys. Res.,* **97,** 8905–8915.

McCaffrey, R., Zwick, P.C., Bock, Y., Prawirodirdjo, L., Genrich, J., Steven, C.W., Puntodewo, S.S.O. & Subarya, C., 2000. Strain partitionining during plate convergence in Northern Sumatra: Geodetic and seismologic constraints and numerical modeling. *J. Geophys. Res.,* **105,** 28 363–28 376.

McQuarrie, N., Stock, J.M., Verdel, C. & Wernicke, B.P., 2003. Cenozoic evolution of Neothetys and implications for causes of plate motions. *Geophys. Res. Lett.,* **30,** doi:10.1029/2003GL017992.

Meissner, R. & Strehlau, J., 1982. Limits of stresses in continental crusts and their relation to the depth-frequency distribution of shallow earthquakes. *Tectonics,* **1,** 73–89.

Mount, V.S. & Suppe, J., 1987. State of stress near the San Andreas fault: Implications for wrench tectonics. *Geology,* **15,** 1143–1146.

Ni, J. & Barazangi, M., 1986. Seismotectonics of the Zagros continental collision and comparison with the Himalayas. *J. geophys. Res.,* **91,** 8205–8218.

Pinet, C., Jaupart, C., Marschol, J.-C., Gariepy, G., Bienfait, G. & Lapointe, R., 1991. Heat flow and structure of the lithosphere in the eastern Canadian shield. *J. geophys. Res.,* **96,** 19 941–19 963.

Platt, J.P., 1993. Mechanics of oblique convergence. *J. geophys. Res.,* **98,** 16 239–16 256.

Pollack, H.N., Hurter, S.J. & Johnson, J.R., 1993. Heat flow from the earth's interior: analysis of the global data set. *Rev. Geophys.,* **31,** 267–280.

Rice, J.R., 1992. Fault stress states, pore pressure distributions, and the weakness of the San Andreas fault. *Fault Mechanics and Transport Properties of Rock*. B.E. a. T.-F. Wong. San Diego, Calif., Academic: 475–503.

Sella, G.F., Dixon, T.H. & Mao, A., 2002. REVEL: A model for recent plate velocities from space geodesy. *J. Geophys. Res.* **107**(B4): 2081, doi:10.1029/2000B000033.

Sibson, R.H., 1982. Fault zone model, heat flow, and the depth distribution of earthquakes in the continental crust of the united states. *Bull. Seism. Soc. Am.,* **72,** 151–163.

Talebian, M. & Jackson, J.A., 2002. Offset on the Main Recent Fault of the NW Iran and implications for the late Cenozoic tectonics of the Arabia-Eurasia collision zone. *Geophys. J. Int.,* **150,** 422–439.

Talebian, M. & Jackson, J.A., 2004. A reappraisal of earthquake focal mechanisms and active shortening in the Zagros mountains of Iran. *Geophys. J. Int.,* **156,** 506–526.

Tatar, M., Hatzfeld, D. & Ghafori-Ashtiany, M., 2004. Tectonics of the Central Zagros (Iran) deduced from microearthquake seismicity. *Geophys. J. Int.,* **156,** 255–266.

Tatar, M., Hatzfeld, D., Martinod, J., Walpersdorf, A., Ghafori-Ashtiany, M. & Chéry, J., 2002. The present-day deformation of the central Zagros from GPS measurements. *Geophys. Res. Lett.,* **29**(19), 1927, doi: 10.1029/2002GL015427.

Teyssier, C. & Tikoff, B., 1998. Strike-slip partitioned transpression of the San Andreas fault system: a lithospheric-scale approach. Continental transpressional and transtensional tectonics. eds Holdsworth, R.E., Strachan, R.A. & Dewey, J.F., London, Geological Society, **135,** 143–158.

Thatcher, W., 1990. Present-day crustal movements and the mechanics of cyclic deformation. The San Andreas Fault system, California. R. E. Wallace. Washington, *Geological Survey Professional Paper*. **1515,** 189–205.

Tikoff, B. & Peterson, K., 1998. Physical experiments of transpressional folding. *J. Structural Geology,* **20,** 661–672.

Townend, J. & Zoback, M.D., 2000. How faulting keeps the crust strong. *Geology,* **28**(5), 399–402.

Tsenn, M.C. & Carter, N.L., 1987. Upper limits of power law creep of rocks. *Tectonophysics,* **136,** 1–26.

Vernant, P. *et al.*, 2004. Contemporary Crustal Deformation and Plate Kinematics in Middle East Constrained by GPS measurements in Iran and Northern Oman. *Geophys. J. Int.,* **157,** 381–398.

Wilcox, R.E., Harding, T.P. & Seely, D.R., 1973. Basic wrench tectonics. *AAPG Bulletin,* **57,** 74–96.